PAPER

Check for updates

Switching microobjects from low to high aspect ratios using a shape-memory effect†

Fabian Friess, [ab] Andreas Lendlein [ID] *[ab] and Christian Wischke [ID] ‡*[a]

Spherical particles from shape-memory polymers (SMP) can be stretched to ellipsoids with high aspect ratio (AR) and temporarily stabilized. They can switch back to low AR upon thermal stimulation. Here, the creation of an alternative shape-switching capability of particles from low to high AR is introduced, where a SMP matrix from polyvinyl alcohol (PVA) is used to create crosslinked high AR particles and to program the embedded micrometer-sized particles from a second SMP (oligo(ε-caprolactone) micronetworks, MN) with a low switching temperature T_{sw}. This programming proceeds through shape-recovery of the PVA matrix, from which the MN are harvested by PVA matrix dissolution. The use of a dissolvable SMP matrix may be a general strategy to efficiently create systems with complex moving capabilities.

1. Introduction

Shape-memory polymers (SMP) can perform predetermined shape-changes upon thermal stimulation.[1] This movement is driven by a gain in entropy. Depending on the stress level created by this effect, a connected secondary object can be moved. In this way, SMP can be used as thermomechanical energy storage systems, which enable self-sufficient devices such as deployable antenna,[2] anti-counterfeit labels,[3] the anchoring of medical implants[4] and the driving of attached propellers.[5] The shape-memory effect (SME) works well in miniaturized objects down to the submicron level. Examples are switchable pillars on microarrays,[6] microfluidic chips,[7] micro-/nanofibers,[8] and particles.[9] Recently, the outer confinement provided by the diameter of nanofibers has been identified as a design parameter to control the shape-memory performance for object diameters lower than 1 μm.[10] SMP particles of different sizes, typically in the lower micrometer size range, which have been prepared so far, consist either of physically crosslinked thermoplastic polymers[9,11–13] or polymers with covalently crosslinked macromolecules.[14–17] The latter particles are named micronetworks (MN). The term MN has been used to differentiate those crosslinked particles from thermoplastic (precursor) microparticles (MP) and emphasizes

the relevance of the network architecture for the switching function of those microobjects.

Starting from spherical particles, discs and prolate ellipsoids can be obtained as temporary particle shapes through compression between hot plates or by stretching after embedding in a suitable film matrix (phantom) such as from polyvinyl alcohol (PVA).[18–21] These particles are supposed to switch back to spheres when the suitable stimulus, typically heat, is applied. For ellipsoids, the aspect ratio (AR; AR = $l \cdot s^{-1}$; l: longest axis; s: shortest axis) of the particles can serve as a quantitative measure of switching efficiency, as it should be decreased to unity when switching is quantitative. While some studies with particles from thermoplastic SMP reported high shape-recovery rates,[12] the shape recovery from ellipsoidal to spherical state was partial in some other materials exclusively based on physical netpoints.[9] This motivated the exploration of covalently crosslinked MN, which demonstrated a quantitative switching ability to AR ∼ 1 when exceeding the thermal transition temperature of the assigned switching domains.[14] Beside direct temperature exposure to induce the SME of SMP materials, also solvent absorption may trigger shape alterations of particles towards a reduced AR e.g. through plasticization and interfacial tension-driven surface area minimization.[22,23] However, it is important to differentiate this phenomenon of viscous flow from the here employed mechanism of entropy-elastic recovery forces stored in and released from polymer network materials.

Realizing the opposite movement from spheres to ellipsoids, *i.e.*, an alternative switching direction (aSME) towards an increased AR, sets higher conceptual challenges. Such phenomena are known for colloidal particles from amphiphilic polymers based on photoinduced isomerization or selective

[a] *Institute of Active Polymers and Berlin-Brandenburg Center for Regenerative Therapies, Helmholtz-Zentrum Hereon, Kantstr. 55, 14513 Teltow, Germany. E-mail: andreas.lendlein@hereon.de, christian.wischke@pharmazie.uni-halle.de*
[b] *Institute of Chemistry, University of Potsdam, Karl-Liebknecht-Str. 25, 14476 Potsdam, Germany*
† Electronic supplementary information (ESI) available. See DOI: 10.1039/d1sm00947h
‡ Current address: Institute of Pharmacy, Martin-Luther-University Halle-Wittenberg, Germany.
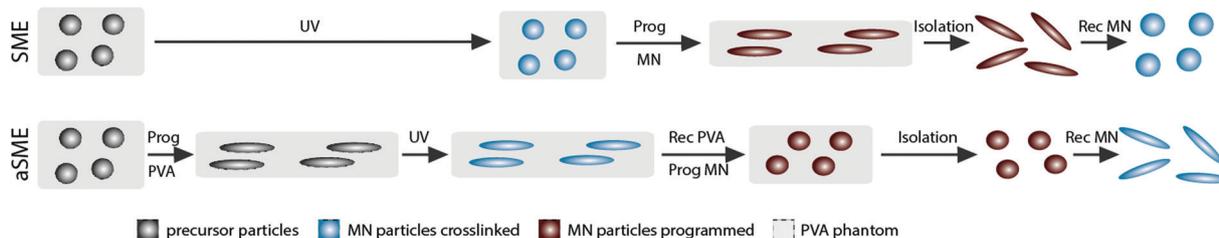
Fig. 1 Principles of creating MN with SME and aSME. Upper panel: For SME, precursor MP (dark grey) are embedded in PVA phantoms (light grey) and crosslinked by UV irradiation to MN defining the permanent shape (blue). By programming *via* phantom stretching, a temporary MN shape (red) with AR ≫ 1 is obtained. After PVA dissolution, shape recovery to AR ~ 1 can be triggered by heat exposure. Lower panel: For aSME, PVA phantoms loaded with precursor particles are first programmed to an elongated state, followed by UV irradiation of the now ellipsoidal precursor particles to create a permanent ellipsoidal MN shape. By shape recovery of the PVA, the MN are simultaneously programmed to AR ~ 1, which later can switch to AR ≫ 1.

swelling.[24,25] In case of SMP particles with an internal MN structure, a synthesis and programming strategy would be required for aSME that enables to first prepare ellipsoids as permanent MN shapes and then allows their controlled and fully aligned deformation to spheres as temporary shapes.

Here, the ability of PVA, known as phantom material with a passive role during conventional shape programming,[21] to be an active material showing a SMP itself[5] was considered as starting point (Fig. 1). Spherical precursor microparticles (MP) based on crosslinkable oligo(ε-caprolactone) (oCL) should be incorporated in the PVA phantom. Instead of being crosslinked to MN in spherical shape after templating as performed in literature[14] and shown in Fig. 1, upper pannel (denoted as SME), an alternative switching feature towards higher AR (denoted as aSME) should be realized by first programming the PVA with embedded MP to an elongated temporary shape with subsequent UV-induced MN synthesis. The MN stay in the PVA matrix during subsequent shape recovery of the PVA. In this way, a programming of the embedded ellipsoidal MN to a temporary spherical shape should be realized (Fig. 1, lower panel), *i.e.* the training of embedded SMP MN particles by the PVA matrix. Particles isolated by PVA dissolution should then be evaluated for their micronetwork structure and shape-switching ability.

2. Experimental

A detailed description of experimental procedures is provided in the ESI.†

Tests for phantom material selection

Solutions of PVA (Mowiol 3–85 [M_n = 5.6 kDa; polydispersity PD = 2.5; degree of deacetylation DD = 85%] or Mowiol 4–88 [M_n = 12.6 kDa; PD = 2.5; DD = 88%], 18 g) in pure water (60 mL, 23 wt%) were pipetted (1.3 mL) into rectangular molds (5 cm × 1.2 cm × 0.3 mm), dried for 24 hours at room conditions followed by detachment from the mold and further drying (60 °C, 4 h). DSC data were collected from the second heating cycle (10–250 °C, 10 K min⁻¹, nitrogen atmosphere; DSC 204 F1, Netzsch). For determining shape-memory properties, phantoms were preheated in the thermochamber (BW91250, Zwick/Roell) of a tensile tester (Z005, Zwick/Roell)

to become more flexible before clamping and were stretched at 30 mm min⁻¹ with a preforce of 1 N. After the maximum elongation was reached (*e.g.*, ε_{ph} = 150%), samples were cooled to room temperature and the shape-fixity rate R_f and shape-recovery rate R_r were calculated according to eqn (S1) and (S2) (ESI†).

Precursor microparticles

A glass capillary microfluidic device was used to prepare microparticles (MP) by a well-controlled emulsification of a 4.53 wt% solution (ethyl acetate : DCM, 1 : 1, v/v) of linear, bifunctional oCL-IEMA (oCL M_n 8 kDa, PD 1.5 (GPC); degree of functionalization 99% (NMR)) in a 2.5 wt% aqueous PVA (Mowiol 4–88) solution. Solvents were removed by evaporation, MP were washed with water, and lyophilized.

Embedding, MN crosslinking and programming in PVA phantoms

A suspension of 1.5% (w/v) MP in 23 wt% aqueous PVA (Mowiol 3–85) were casted in molds (6.8 cm × 2.3 cm), dried first at r.t. for 24 h and then at 60 °C for 4 h. For crosslinking, UV light (250–450 nm, I = 80 mW cm⁻²) of an Omnicure 2000 lamp (IGB-Tech, Germany) was directed at the center of the sample inside the thermochamber of the tensile tester with a single-pole light guide (Fig. S4, ESI†). For SME, the phantoms were (i) preheated to the programming temperature (T_{prog} = 65 °C) and clamped, (ii) UV irradiated for 20, 40 or 60 min, (iii) stretched at 30 mm min⁻¹ with a preforce of 1 N to an elongation of ε_{ph} = 150%, (iv) cooled to room temperature allowing crystallization of the crosslinked MN for fixation of their ellipsoidal temporary shape. Subsequently, (v) the MN were harvested by dissolving the PVA-matrix and were purified similar to MP as described above. For aSME, the UV-irradiation and PVA deformation steps were inversed, *i.e.* preheating (i) was followed by (ii) phantom programming (30 mm min⁻¹, preforce 1 N, ε_{ph} = 150%, $T_{prog\,PVA}$ = 65 °C) and (iii) crosslinking of the now molten ellipsoidal precursor droplets by UV-irradiation. After (iv) the cooling step, (v) the samples were exposed to $T_{rec\,PVA} = T_{prog\,MN}$ = 100 °C in an oven to allow shape recovery of the PVA phantom and simultaneous programming of MN towards lower *AR*, which were fixed by cooling to r.t. outside the oven. Step (vi) involved MN harvesting by PVA dissolution and purification.

Analysis of MP/MN

The conversion of IEMA groups was determined from purified MN (powder) by ATR-FTIR-spectroscopy (Nicolet 6700, Thermo Scientific). DSC data were collected from the second heating cycle (-100 to $+150$ °C, 10 K min^{-1}, nitrogen atmosphere). Laser diffraction (Mastersizer 2000, Malvern) was performed in water for MP and in DCM for pre-swollen MN, where scattering artefacts were excluded when determining the volume-weighted mean diameter $D[4, 3]$. For solvent triggered shape switching, DCM was added to programmed MN deposited on a glass slide and later evaporated, while continuously monitoring particle shape by light microscopy (DMI 6000B, Leica). Thermally-induced SME and aSME was studied for aqueous dispersions of MN in a closed heating chamber at a heating rate of 10 K min^{-1} (LTS 350 stage chamber, Lincam) by light microscopy (Axio Imager.A1m, Carl Zeiss) from 35 to 70 °C with time-lapse imaging (1 image per 0.5 K). The images were evaluated for particle AR with the ImageJ particle analyzing tool (V1.46r, National Institute of Health, USA).

3. Results and discussion

3.1 Selection of phantom material with active shape-switching capability

One essential requirement to realize the concept as summarized in Fig. 1 is a high shape recovery rate of PVA. While some previous work illustrated a temperature- or solvent-induced SME of covalently crosslinked PVA or PVA composites,[26–28] which, however, may not or at least not easily dissolve in water, here the use of easily water soluble PVA was essentially required for later isolation of particulate inclusions from PVA phantoms. PVA is derived from polyvinyl acetate by partial deacetylation (degree of deacetylation, DD). Since low number-average molecular weight M_n and a DD of 80–90% are associated with high aqueous solubility at ambient conditions,[29] the following materials were investigated: PVA 3–85 (M_n = 5.6 kDa; polydispersity PD = 2.5; DD = 85%) and PVA 4–88 (M_n = 12.6 kDa; PD = 2.5; DD = 88%). In order to explore the potential shape-switching capacity, PVA films were prepared by casting aqueous PVA solutions with subsequent drying. Thermal analysis illustrated that both PVA materials showed a glass transition temperature (T_g, point of inflection in DSC thermogramm) of amorphous domains close to 70 °C and a melting transition temperature (T_m) of crystalline domains at 163 °C (Fig. 2A), which may serve as temporary and permanent netpoints, respectively, for the SME.

To evaluate the shape-memory capabilities of pure PVA-phantoms, cyclic thermomechanical tests were conducted. The samples were heated to the respective programming temperatures T_{prog} (60, 70, or 80 °C), stretched to defined phantom elongations ε_{ph} (50, 100, 150, or 250%), fixed in their temporary shape by cooling at constant strain, and analyzed for their shape recovery by heating to 80 °C or 100 °C. All PVA samples exhibited a SME (Fig. 2B). While the shape fixity rate R_f was always virtually 100% (measure of the capability to fix the
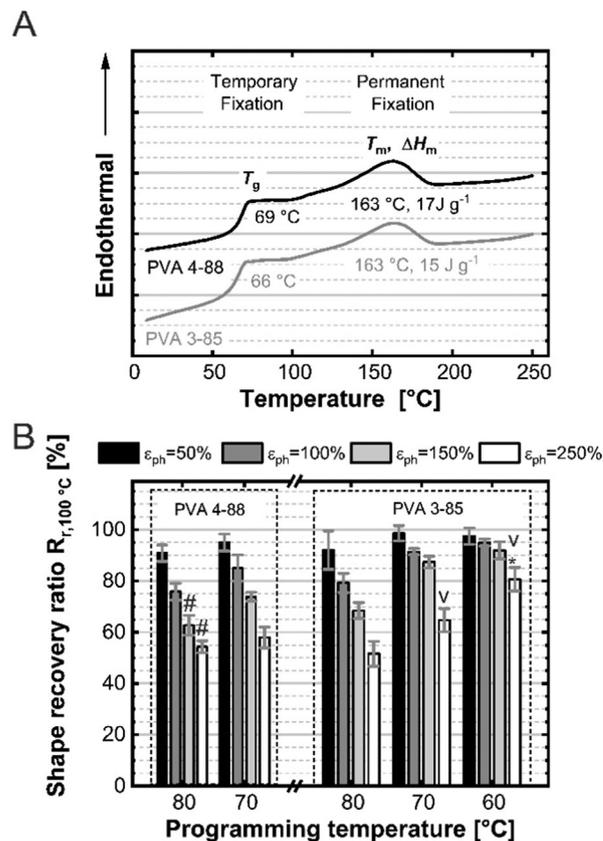

Fig. 2 Exploring the SME of PVA. (A) Thermal properties of PVA as determined by dynamic scanning calorimetry (DSC) in the second heating run (endotherms are shifted along y-axis for better readability). (B) Shape-recovery ratio R_r at 100 °C depending on T_{prog} and phantom elongation ε_{ph} (mean, S.D.; n = 4–10, *n = 3, #n = 2; ^{v} high tendency to break).

deformation strain applied during programming; see ESI,† Fig. S1), the shape recovery rate R_r systematically decreased with increasing programming temperature and increasing ε_{ph} (further data see ESI,† Fig. S2 and S3). This might be assigned to a slipping of PVA crystallites with increasing ε_{ph} or their partial melting at elevated T_{prog}, which affects the capability of PVA crystallites to act as permanent netpoints, i.e. to fix the permanent shape. Based on this analysis, phantoms from PVA 3–85 with ε_{ph} = 150% and T_{prog} at 65 °C, i.e. close to T_g, was selected for further experiments.

3.2 Micronetwork synthesis and properties

Precursor MP should be prepared for later embedding in PVA phantoms. Polymer solutions of linear oligo(ε-caprolactone) (oCl; number-average molecular weight 8 kDa) bearing photo-crosslinkable 2-isocyanatoethyl methacrylate (IEMA) endgroups were templated into droplets by microfluidic emulsification in a glass capillary device in the dripping mode. After solvent evaporation, monodisperse precursor MP of 16.8 µm were obtained.[30]

These precursor MP were embedded in PVA phantoms to subsequently conduct, in variable orders, mechanical deformation and UV-irradiation for photocrosslinking of IEMA moieties

(for images see Fig. S4, ESI†). For MN with SME functionality (Fig. 1, upper panel), irradiation was applied first to the spherical MP inclusion, thus fixing the formed MN structure in a permanent spherical shape. Subsequently, phantom stretching was performed for MN programming at $T_{MN\text{-}Prog}$ = 65 °C. For aSME, the PVA phantoms were first deformed (programmed) at $T_{PVA\text{-}Prog}$ = 65 °C and then irradiated to create MN with a permanent ellipsoidal shape. The programming of these MN to a temporary shape of AR ∼1 was conducted by elastic shape-recovery of the PVA phantom at $T_{PVA\text{-}Rec}$ = $T_{MN\text{-}Prog}$ = 100 °C (Fig. 1, lower panel). In all cases, the temporary shape of the particles was fixed by cooling. The PVA phantoms were subsequently dissolved to collect the programmed MN.

During this procedure, UV-irradiation for micronetwork synthesis by oCL-IEMA crosslinking was performed at T_{cross} = 65 °C in the thermochamber of the tensile tester. Under these conditions, the (particulate) oCL inclusions were in the molten state to ensure sufficient chain mobility for homogeneous network formation. UV-irradiation was performed without photoinitiators for 20, 40 or 60 min (λ = 250–450 nm, I = 80 mW cm^{-2}), as indicated in the sample codes (e.g. SME60 or aSME60 for MN particles synthesized with 60 min irradiation).

The effective formation of covalent netpoints is essential to define the permanent shape of MN and thus to enable their shape-switching capability. Increasing irradiation times (20–60 min) of particle-loaded phantoms resulted in overall increasing conversion of IEMA moieties as confirmed by FTIR analysis (Fig. 3A; ∼100% signal decay at 815 cm^{-1} after 60 min irradiation). The DSC analysis of the melting transitions associated with crystalline oCL domains of MN showed a new and increasing T_m signal at ∼46 °C (Fig. 3B) with increasing irradiation time, which is shifted to lower temperatures relative to the melting transition of the oCL-IEMA precursor. This illustrates a restricted chain mobility for crystallite growth

and confirms both the oCL chain incorporation in a polymer network structure and the presence of crystalline domains as required for fixation of the temporary MN shape. Also after 60 min of crosslinking, apparently a certain fraction of crystallites with higher T_m were remaining in the MN samples. This observation might indicate the presence of chain segments in the MN that are not restricted in mobility (dangling chains) and/or the admixture of a small portion of not fully crosslinked particles, such as from the edges of the phantoms that possibly have been exposed to lower intensities of UV irradiation.

A covalent polymer network structure represents an indefinitely large molecule, which is not soluble, but can swell in good solvents adapting a larger volume without disintegration. Particle size analysis of spherical precursor MP by laser diffraction showed a very narrow size distribution with diameters of 16.8 μm (Fig. 3C). As exemplarily demonstrated for three independently crosslinked SME60 MN batches based on those precursor MP, the MN particles did not dissolve when exposed in dichloromethane (DCM) as a good swelling agent. Instead, they adopted a swollen state with diameters of about 27 μm (26.8 μm, 26.9 μm, 27.1 μm). Based on these data, a volumetric degree of swelling Q of 410 ± 5% could be concluded. Overall, the analysis confirmed the successful and reproducible MN synthesis.

3.3 Switching functions of MN with SME and aSME

SME and aSME MN particles differ in their permanent shape, which is the state of lowest internal stress. This relaxed state will be adapted through entropy elasticity of the polymer network if physical interactions such as glassy domains or polymer crystallites are removed that hinder the movement of strained chain segments.

Considering the swellability of non-programmed MN particles as evaluated above by laser diffraction, solvent exposure is one approach to enable high chain mobility. Starting here from dry programmed particles in their temporary shape
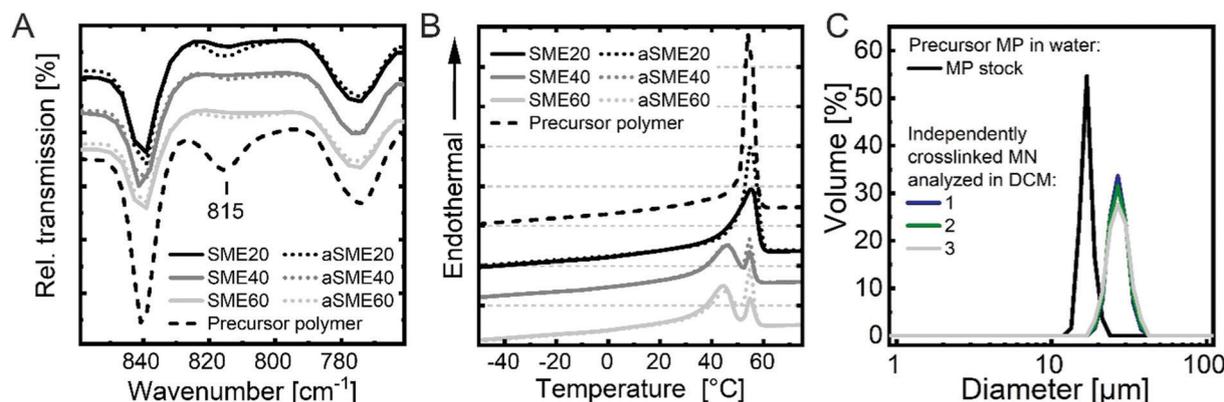

Fig. 3 Evaluation of successful MN synthesis at different UV illumination conditions and resulting material properties. (A) IEMA conversion (decay of =CH$_2$ out of plane bending, 815 cm^{-1}) depending on irradiation time (20, 40, or 60 min). (B) Shift of T_m depending on irradiation time (20, 40, or 60 min). The curves in (A) and (B) represent the mean of n = 2–4 independent MN samples (programmed) and are shifted along the y-axis for better readability. (C) Exemplary particle size analysis by laser diffraction of crosslinked MN particles (SME60; three independently crosslinked batches) in swollen state (in DCM) relative to the corresponding non-swollen precursor particles (MP in water) to show successful crosslinking. Data are presented as volume-weighted mean diameter D[4, 3].
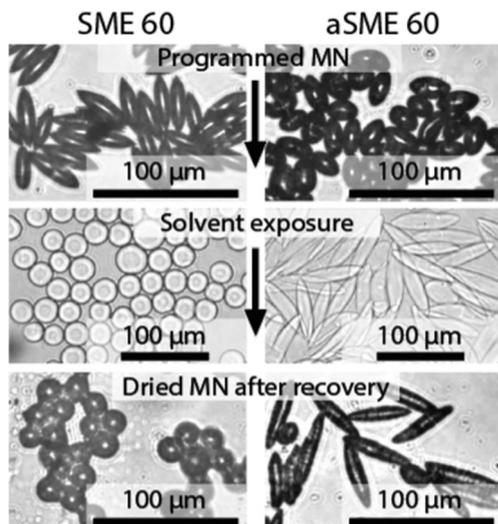
Fig. 4 Solvent triggered removal of temporary crystalline netpoints and corresponding shape switching of SME and aSME to spherical and ellipsoidal permanent shapes, respectively. Exemplary images for SME60 and aSME60 MN (SME: $T_{prog\,MN}$ = 65 °C; aSME: $T_{rec\,PVA}$ = $T_{prog\,MN}$ = 100 °C).
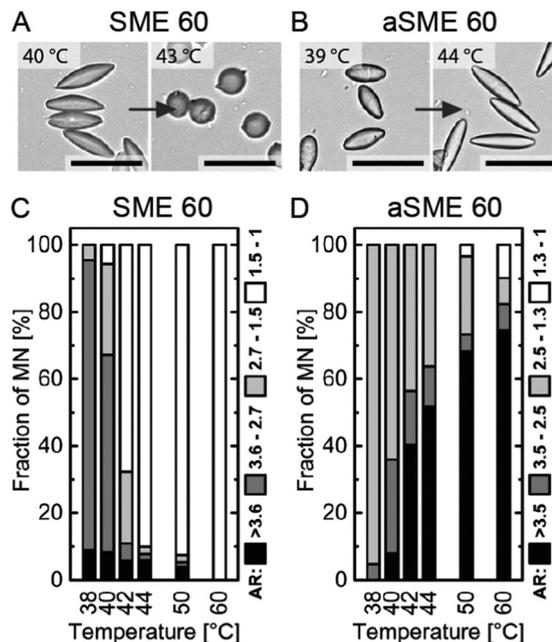

Fig. 5 Analysis of thermally-induced SME and aSME of MN. Exemplary light microscopic images for (A) SME60 and (B) aSME60 particles. (C and D) Quantitative analysis of shape recovery. The kinetics of shape switching are shown by the relative fraction of MN of a given AR range at different temperature steps throughout a continuous heating experiment. The number of MN analyzed at a temperature (*n*) were *n* = 195–258 for SME and *n* = 51–64 for aSME. Scale bars in (A and B) denote 50 µm.

(SME: AR > 3; aSME: AR ∼ 2), light microscopy illustrated that the solvent DCM triggered the shape shifts to the anticipated permanent shapes (SME: spheres with AR = 1; aSME: spindle-like ellipsoidal shape with AR > 4) (Fig. 4). Spatially directed swelling of certain lyophilic domains is a possible cause of shape alteration in patchy or lamella-like amphiphilic particle systems,[31,32] which would be reversed during solvent removal. Here, however, the principle of shape shifts towards higher AR for aSME MN was confirmed as a solvent-triggered chain relaxation that was not effected by solvent removal.

In order to study the thermally-induced SME and aSME, which now should be triggered in a purely aqueous environment, samples were studied on the heating stage of a light microscope. Fig. 5A (Movie S1, ESI†) illustrated a clear shift from ellipsoidal towards spherical shape, *i.e.* to decreasing AR, for SME MN prepared by the conventional programming process. In contrast, when facilitating the SME of PVA phantoms to program aSME MN, the proposed switching towards increased AR was confirmed (Fig. 5B and Movie S2, ESI†). A quantitative description of the switching was obtained by image analysis, where the MN were categorized in different AR fractions for better visualization (Fig. 5C and D; for individual data see Fig. S5, ESI†). It was observed that not always all particles of a sample behaved identically, which may be due to local differences of MN crosslinking at different positions in the phantom in the given experimental set-up. Light focusing on the center of the phantom with potentially lower intensities at the edges, light scattering by embedded MN during UV irradiation, possibly nano-sized gas bubbles trapped in the PVA phantom, or an influence of oxygen on the radical reaction might potentially have contributed to this phenomenon. Anyhow, the kinetic analysis (Fig. 5C and D) clearly indicated the temperature-dependency and functionality of the shape switch

towards lower and higher AR for SME and aSME, respectively, thus confirming the hypothesis of this study.

Generally, the extent of relative increase of AR during the aSME is largely influenced by the capacity of the PVA phantom to deform inclusions during elastic phantom recovery (Fig. 1). It has to be emphasized that the local displacement communicated from the macroscopic phantom to the individual particulate inclusion is affected be several parameters besides the shape-memory properties of the PVA, which were excellent at the selected conditions (Fig. 2B). Relevant aspects are, *e.g.*, the mechanical properties of the MN compared to the PVA phantom at the given temperature. Accordingly, the relative alteration of AR during shape switching of aSME may be further modified in the future by increasing the displacement during programming of MNs, *e.g.* by reducing the mechanical strength of the MNs (altered oCL precursor, lower crosslink density) to an extent that would not yet result in network damage during programming, by increasing the strength of phantoms using PVA with different M_n and DD, or by further modification of the thermo-mechanical programming protocols. Additionally, the conditions of polymer network synthesis may be altered. For example, a reduced UV exposure time of 20 min resulted in less crosslinked and thus softer MN (aSME20), which adapted temporary shapes of lower AR during aSME programming (see Fig. S6 *vs.* Fig. S5, ESI†).

As typical for chemically crosslinked, thermosensitive SMP, the SME is a one way/one time effect. Reprogramming can be

challenging particularly for aSME particles, *e.g.* considering the required aligned embedding in stretched phantoms.

4. Conclusions

This study illustrated that a spatially directed shape-switch of oCL-based shape-memory polymer micronetworks with covalent netpoints is not restricted to shifting from ellipsoids to spheres. Instead, also an alternative switching of particle shape to higher AR can be realized by a suitable programming process that utilizes the SME of the PVA matrix, in which the MN are embedded. The here demonstrated ability of particles to switch on-demand to an increased AR and, thus, an increased surface area may be useful to occlude microfluidic channels, provide enhanced surfaces for adsorption of target substances or perforate *e.g.* tumor cells after particle engulfment. Beyond that, the SMP programming concept introduced here may become a general strategy to efficiently and in parallel create systems with complex moving capabilities also for other materials, switching directions and types of microobjects.

Conflicts of interest

There are no conflicts of interest to declare.

Acknowledgements

References

1 A. Lendlein and O. E. C. Gould, *Nat. Rev. Mater.*, 2019, **4**, 116–133.
2 S. Jape, M. Garza, J. Ruff, F. Espinal, D. Sessions, G. Huff, D. C. Lagoudas, E. A. Peraza Hernandez and D. J. Hartl, *Smart Mater. Struct.*, 2020, **29**, 115011.
3 C. J. Leverant, S.-Y. Leo, M. A. Cordoba, Y. Zhang, N. Charpota, C. Taylor and P. Jiang, *ACS Appl. Polym. Mater.*, 2019, **1**, 36–46.
4 G. I. Peterson, A. V. Dobrynin and M. L. Becker, *Adv. Healthcare Mater.*, 2017, **6**, 1700694.
5 J. Yuan, W. Neri, C. Zakri, P. Merzeau, K. Kratz, A. Lendlein and P. Poulin, *Science*, 2019, **365**, 155–158.
6 J. Wang, Q. Zhao, H. Cui, Y. Wang, H. Chen and X. Du, *J. Mater. Chem. A*, 2018, **6**, 24748–24755.
7 M. Ebara, K. Uto, N. Idota, J. M. Hoffman and T. Aoyagi, *Soft Matter*, 2013, **9**, 3074–3080.
8 F. Zhang, Z. Zhang, T. Zhou, Y. Liu and J. Leng, *Front. Mater.*, 2015, **2**, 62.
9 C. Wischke, M. Schossig and A. Lendlein, *Small*, 2014, **10**, 83–87.
10 T. Sauter, K. Kratz, M. Heuchel and A. Lendlein, *Mater. Des.*, 2021, **202**, 109546.
11 L. M. Cox, J. P. Killgore, Z. Li, R. Long, A. W. Sanders, J. Xiao and Y. Ding, *Langmuir*, 2016, **32**, 3691–3698.
12 Q. Y. Guo, C. J. Bishop, R. A. Meyer, D. R. Wilson, L. Olasov, D. E. Schlesinger, P. T. Mather, J. B. Spicer, J. H. Elisseeff and J. J. Green, *ACS Appl. Mater. Interfaces*, 2018, **10**, 13333–13341.
13 Y. K. Bai, J. W. Zhang, J. P. Ju, J. M. Liu and X. Chen, *React. Funct. Polym.*, 2020, **157**, 104770.
14 F. Friess, U. Nochel, A. Lendlein and C. Wischke, *Adv. Healthcare Mater.*, 2014, **3**, 1986–1990.
15 S. M. Brosnan, A.-M. S. Jackson, Y. Wang and V. S. Ashby, *Macromol. Rapid Commun.*, 2014, **35**, 1653–1660.
16 J. Huang, L. Lai, H. Chen, S. Chen and J. Gao, *Mater. Lett.*, 2018, **225**, 24–27.
17 C. H. Zhou, Y. R. Ni, W. T. Liu, B. Tan, M. C. Yao, L. Fang, C. H. Lu and Z. Z. Xu, *Macromol. Rapid Commun.*, 2020, **41**, 2000043.
18 M. Nagy and A. Keller, *Polym. Commun.*, 1989, **30**, 130–132.
19 A. C. Courbaron, O. J. Cayre and V. N. Paunov, *Chem. Commun.*, 2007, 628–630.
20 J. A. Champion, Y. K. Katare and S. Mitragotri, *Proc. Natl. Acad. Sci. U. S. A.*, 2007, **104**, 11901–11904.
21 C. Wischke and A. Lendlein, *Langmuir*, 2014, **30**, 2820–2827.
22 K. J. Lee, J. Yoon, S. Rahmani, S. Hwang, S. Bhaskar, S. Mitragotri and J. Lahann, *Proc. Natl. Acad. Sci. U. S. A.*, 2012, **109**, 16057–16062.
23 H. G. Wang, B. H. Li, A. G. Yodh and Z. X. Zhang, *Angew. Chem., Int. Ed.*, 2016, **55**, 9952–9955.
24 Y. Li, Y. He, X. Tong and X. Wang, *J. Am. Chem. Soc.*, 2005, **127**, 2402–2403.
25 J. Lee, K. H. Ku, C. H. Park, Y. J. Lee, H. Yun and B. J. Kim, *ACS Nano*, 2019, **13**, 4230–4237.
26 H. Y. Du and J. H. Zhang, *Soft Matter*, 2010, **6**, 3370–3376.
27 Q. M. Bai, G. Z. Zhang, B. Xu, X. Q. Feng, H. Y. Jiang and H. J. Li, *RSC Adv.*, 2015, **5**, 91213–91217.
28 L. Yang, Z. Wang, G. Fei and H. Xia, *Macromol. Rapid Commun.*, 2017, **38**, 1700421.
29 *Polyvinyl alcohol: Developments*, ed. C. A. Finch, John Wiley & Sons, Chichester, 1992.
30 F. Friess, T. Roch, B. Seifert, A. Lendlein and C. Wischke, *Int. J. Pharm.*, 2019, **567**, 118461.
31 X. Zheng, M. Liu, M. He, D. J. Pine and M. Weck, *Angew. Chem., Int. Ed.*, 2017, **56**, 5507–5511.
32 D. Klinger, C. X. Wang, L. A. Connal, D. J. Audus, S. G. Jang, S. Kraemer, K. L. Killops, G. H. Fredrickson, E. J. Kramer and C. J. Hawker, *Angew. Chem., Int. Ed.*, 2014, **53**, 7018–7022.